


The role of fission in mass sensitivity study of the r -process*

Yi Wei Hao (郝艺伟)^{1,2}  Yi Fei Niu (牛一斐)^{1,2†} Zhong Ming Niu (牛中明)³

¹Frontier Science Center for Rare Isotope, Lanzhou University, Lanzhou 730000, China

²School of Nuclear Science and Technology, Lanzhou University, Lanzhou 730000, China

³School of Physics and Optoelectronic Engineering, Anhui University, Hefei 230601, China

Abstract: A sensitivity study was performed to investigate the impact of individual nuclear masses on r -process rare-earth peak abundances in different astrophysical scenarios. The most impactful nuclei are primarily distributed in two regions on the nuclear chart: one located 20-30 neutrons away from stability (defined as region I) and another 7-15 neutrons away from stability (defined as region II), as previously reported in Phys. Lett. B 844, 138092 (2023). In this study, we extend our analysis by focusing on the role of fission in the mass sensitivity study. The results show that, in astrophysical scenarios involving fission, the sensitivity of nuclei in region I is diminished owing to the deposition of a large number of fission fragments in the rare-earth mass region. However, nuclei in region II retain high sensitivity because the contribution of fission decreases in the later stages of nucleosynthesis. This study highlights the impact of fission on the sensitivity of r -process abundances to nuclear masses and enhances the understanding of the rare-earth peak formation mechanism.

Keywords: r -process, rare-earth peak, nuclear mass, fission

DOI: 10.1088/1674-1137/adfe55

CSTR: 32044.14.ChinesePhysicsC.50014106

I. INTRODUCTION

The rapid neutron-capture process (r -process) is a fundamental mechanism in astrophysical nucleosynthesis that is responsible for producing approximately half of the elements that are heavier than iron. This process occurs in extreme astrophysical environments with high neutron fluxes, enabling nuclei to undergo successive neutron captures before decaying back to stability [1]. Observations of metal-poor stars and meteorites have revealed the characteristic abundance patterns of the r -process, highlighting its crucial role in cosmic chemical evolution [2]. However, despite decades of research, the exact astrophysical sites that are responsible for the r -process remain uncertain.

To unravel the origin of r -process elements, theoretical simulations of the nucleosynthesis process are necessary and rely on two essential input components: astrophysical conditions and nuclear properties. Both aspects introduce significant uncertainties. The astrophysical conditions, such as the neutron flux, expansion timescale, temperature, and density evolution, all affect the nucleosynthesis outcomes [3, 4]. Meanwhile, the nuclear properties of neutron-rich isotopes, such as masses, β -decay

rates, neutron capture rates, fission rates, and fission yields, remain largely unmeasured and must be inferred from theoretical models, but these predictions often diverge [5–10]. These uncertainties hinder precise modeling of the r -process and complicate the interpretation of observed abundance patterns.

One unresolved question in r -process nucleosynthesis is the formation mechanism of the rare-earth peak around mass number $A \sim 165$. Unlike the second and third r -process peaks, which are associated with closed neutron shells, the rare-earth peak is believed to originate from other nuclear structure effects [1, 11, 12]. The rare-earth peak could serve as a diagnostic tool for constraining astrophysical conditions of the r -process if its formation was well understood [13]. However, owing to the large uncertainties in nuclear physics inputs, the abundance patterns obtained from r -process simulations exhibit large variance bands that exceed the peak itself, making it difficult to distinguish the abundance patterns produced by different astrophysical environments [6, 14–16]. To improve the reliability of such constraints, reducing the uncertainties in nuclear physics inputs is necessary.

As it is challenging to measure the nuclear properties

Received 31 March 2025; Accepted 18 August 2025; Published online 19 August 2025

* This work was supported by the "Young Scientist Scheme" of National Key Research and Development (R&D) Program (2021YFA1601500), the National Natural Science Foundation of China (12075104, 12447168, 12447106, 11875070, 11935001, 12375109), the China Postdoctoral Science Foundation (2025M773346), the Lingchuang Research Project of China National Nuclear Corporation (CNNC-LCKY-2024-082), the Fundamental Research Funds for the Central Universities (lzujbky-2023-stlt01), the Anhui project (Z010118169), and the Key Research Foundation of Education Ministry of Anhui Province (2023AH050095)

† E-mail: niuyf@lzu.edu.cn

©2026 Chinese Physical Society and the Institute of High Energy Physics of the Chinese Academy of Sciences and the Institute of Modern Physics of the Chinese Academy of Sciences and IOP Publishing Ltd. All rights, including for text and data mining, AI training, and similar technologies, are reserved.

of a large number of neutron-rich nuclei experimentally, sensitivity studies provide an effective approach to pinpoint the key nuclei that have a significant impact on r -process abundances [6, 14–23]. Previous sensitivity studies have primarily focused on the global effects on the abundance distributions caused by mass variations, whereas the specific nuclei that affect the rare-earth peak formation remain unclear. Hence, we performed sensitivity studies specifically targeting the rare-earth peak formation by individually modifying the nuclear masses in the relevant region. We found that the nuclei that have the most significant influence on the rare-earth peak are mainly distributed in two regions, as previously reported in Ref. [24]. However, in astrophysical scenarios in which a large number of fission events occur, the high sensitivity of nuclei lying along the r -process freeze-out path is diminished.

The present paper accompanies Ref. [24]. In this study, we extended our analysis by focusing on the role of fission in studying the sensitivity of r -process abundances to nuclear masses. We analyzed the reasons for the different distribution patterns of nuclei with high sensitivity under different astrophysical scenarios in detail. Our results highlight the impact of fission in shaping the rare-earth peak abundances and enhance the understanding of the rare-earth peak formation mechanism as well as improve its effectiveness as a diagnostic for the r -process site.

II. r -PROCESS CALCULATIONS

The nuclear network NucNet [25] was used to simulate r -process nucleosynthesis. This network includes over 6000 isotopes, covering nuclei with atomic numbers $Z \leq 102$. We obtained the nuclear masses from the finite-range droplet model [26]. The neutron-capture rates were calculated using the publicly available statistical model code TALYS [27]. The β -decay rates were obtained from the JINA REACLIB database [28]. Fission was included as in Ref. [29].

The r -process calculations were performed using a parameterized trajectory, as implemented in Refs. [12, 13], in which the density as a function of time is given by

$$\rho(t) = \rho_1 \exp(-t/\tau) + \rho_2 \left(\frac{\Delta}{\Delta + t} \right)^n, \quad (1)$$

where $\rho_1 + \rho_2$ is the density at time $t = 0$, τ is the expansion timescale, and Δ is a constant real number. The parameter n sets the thermodynamic behavior of the evolution at the late stage of the r -process. For this work, we selected three distinct astrophysical scenarios: (1) a hot wind r -process with entropy $150 k_B$, $Y_e = 0.3$, $\tau = 20$ ms, and $n = 2$; (2) a hot wind r -process with entropy $233 k_B$, $Y_e = 0.1$, $\tau = 35$ ms, and $n = 2$; and (3) a cold wind r -pro-

cess with entropy $150 k_B$, $Y_e = 0.2$, $\tau = 20$ ms, and $n = 6$. In all scenarios, nucleosynthesis calculations started at an initial temperature $T = 10$ GK. We labeled these three trajectories as *hot1*, *hot2*, and *cold*, respectively.

In the *hot1* scenario, fission played a negligible role in nucleosynthesis owing to fewer neutrons in the environment, which prevented significant production of fissioning nuclei. In contrast, both the *hot2* and *cold* scenarios enabled the formation of a substantial number of fissioning nuclei, leading to the deposition of numerous fission fragments in the $A = 110 \sim 170$ region. This is based on the GEF fission fragment distribution model [30], which predicts that fission yields in the neutron-rich regions exhibit both symmetric and asymmetric components [29, 31]. To isolate the effects of fission without direct contributions from fission fragments to the rare-earth peak, we conducted an additional set of simulations under the *cold* scenario. In these simulations, we imposed a simple symmetric split for fission product distributions, ensuring that the fission fragments mainly populated the $A \sim 130$ peak region instead of the rare-earth peak. This specific set of simulations is referred to as the *cold-sym* trajectory in the following discussion.

Following previous sensitivity studies [14, 18], we varied the mass of a single nucleus by ± 1 MeV for 414 nuclei relevant to rare-earth peak formation [12]. For each variation, an abundance pattern was calculated and compared with the baseline using the sensitivity measure F :

$$F = 100 \sum_{A=150}^{178} \frac{|Y_{+1}(A) - Y_{\text{ori.}}(A)| + |Y_{-1}(A) - Y_{\text{ori.}}(A)|}{Y_{\text{ori.}}(A)}, \quad (2)$$

where $Y_{\text{ori.}}(A)$ is the baseline abundance, and $Y_{+1}(A)$ and $Y_{-1}(A)$ are the abundances of the simulations in which a single nuclear mass is increased or decreased by 1 MeV, respectively. When $Y_{\text{ori.}}(A)$, $Y_{+1}(A)$, and $Y_{-1}(A)$ are considered as the final abundances, the corresponding F -values can be found in Ref. [24]. In the present study, we further computed the sensitivity measure $F_{\text{freeze-out}}$ of the abundance distribution at freeze-out with respect to nuclear mass variations, where $Y_{\text{ori.}}(A)$, $Y_{+1}(A)$, and $Y_{-1}(A)$ refer to the abundances at the time of the r -process freeze-out. This allowed us to better understand how nuclear mass variations influence the abundance evolution prior to the onset of decay back to stability.

III. RESULTS AND DISCUSSION

Previous studies [11, 12] have suggested that the formation of the rare-earth peak occurs during the decay back to stability after the r -process freeze-out. In our earlier work [24], we further clarified that the rare-earth peak forms within the time interval between the r -pro-

cess freeze-out and the point when the neutron capture timescale (τ_{ny}) becomes approximately three times longer than the β -decay timescale (τ_β). At this moment, when $\tau_{ny} \approx 3\tau_\beta$, the rare-earth peak abundances are already close to their final values, indicating that the peak has essentially formed. The nuclei that have the most significant influence on the rare-earth peak are mainly distributed in two regions. Region I, located 20–30 neutrons away from stability, corresponds to the position of the nuclear flow at the r -process freeze-out. Region II, 7–15 neutrons away from stability, aligns with the r -process path at the point of $\tau_{ny} \approx 3\tau_\beta$.

Figure 1 shows the distribution of nuclei with high sensitivity measure F under different astrophysical scen-

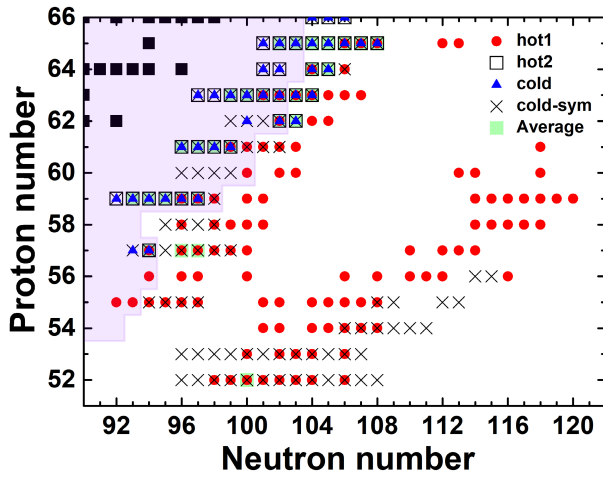


Fig. 1. (color online) Distribution of nuclei with a sensitivity measure F greater than 200 in the *hot1*, *hot2*, *cold*, and *cold-sym* scenarios. The region of measured nuclear masses from AME2020 [32] is overlaid with a pink color and the solid black squares are stable isotopes. The data of the sensitivity measure F in four different scenarios were obtained from Ref. [24]. The top 30 nuclei with the largest averaged sensitivity F values across the *hot1*, *hot2*, and *cold* scenarios are indicated by light green shaded squares.

arios, with the sensitivity data in four different scenarios obtained from Ref. [24]. As a supplement to this analysis, we further calculated the average sensitivity measure F across the *hot1*, *hot2*, and *cold* scenarios. The top 30 nuclei with the largest averaged sensitivity F values are listed in Table 1 and indicated by light green shaded squares in Fig. 1. It is evident that the nuclei with the highest averaged sensitivity values were primarily located in region II, because these nuclei exhibited consistently high sensitivity across multiple astrophysical scenarios. In contrast, region I contained only one nucleus, ^{152}Te , with a relatively high averaged sensitivity. Although the sensitivity measure F of ^{152}Te was low under the *hot2* and *cold* scenarios, its exceptionally high sensitivity under the *hot1* scenario resulted in a large average F value.

In the scenarios considered in this study, the equilibrium phases were maintained at the time of the r -process freeze-out. Thus, the final abundances were expected to be sensitive to changes in the masses of nuclei located along the r -process freeze-out path, as explained in detail in our previous work [24]. However, in the *hot2* and *cold* scenarios, the nuclei in region I exhibited lower F values, indicating that mass variations in this region had little or no impact on the final abundance distribution.

Nevertheless, we found that mass variations of certain nuclei in region I could lead to significant differences in the abundance pattern at the time of the r -process freeze-out, as shown in Fig. 2. We selected two nuclei from region I as examples. In the *hot1* scenario, the mass variation of ^{152}Te resulted in a noticeable difference in the abundance distribution at the freeze-out time. In the *cold* scenario, the mass variation of ^{172}Ba also led to significant differences at freeze-out. However, compared with the *hot1* case, the overall abundance in the rare-earth peak region was much lower. The situation in the *hot2* scenario was similar to that in the *cold* scenario. To quantify the sensitivity of the abundance distribution at freeze-out time to nuclear masses, we calculated the sensitivity measure $F_{\text{freeze-out}}$, which reflects how mass variations influence the abundance pattern at freeze-out. The

Table 1. The 30 most important nuclei with the highest averaged sensitivity measures F were obtained by averaging the F values across the *hot1*, *hot2*, and *cold* scenarios. An asterisk denotes a nucleus with experimental mass data in the AME2020 mass table [32]. A detailed list of the nuclei with the highest sensitivity under each astrophysical scenario is available in Ref. [24].

Average														
Z	A	F	Z	A	F	Z	A	F	Z	A	F	Z	A	F
64	168	412.73	63	165	348.09*	65	168	301.85*	63	163	273.11*	65	167	233.27*
63	166	396.32	61	159	317.41*	57	153	301.48	59	156	268.38*	52	152	232.14
65	170	386.57	62	164	315.41*	59	155	296.77*	59	154	265.96*	59	152	229.16*
63	164	377.39*	65	172	312.50	65	171	295.67	63	162	259.27*	59	153	222.69*
65	169	376.35	61	158	306.86*	65	173	282.38	57	151	245.65*	62	165	220.96
63	167	349.18	64	169	306.86	57	154	273.65	61	160	240.01*	61	157	220.32*

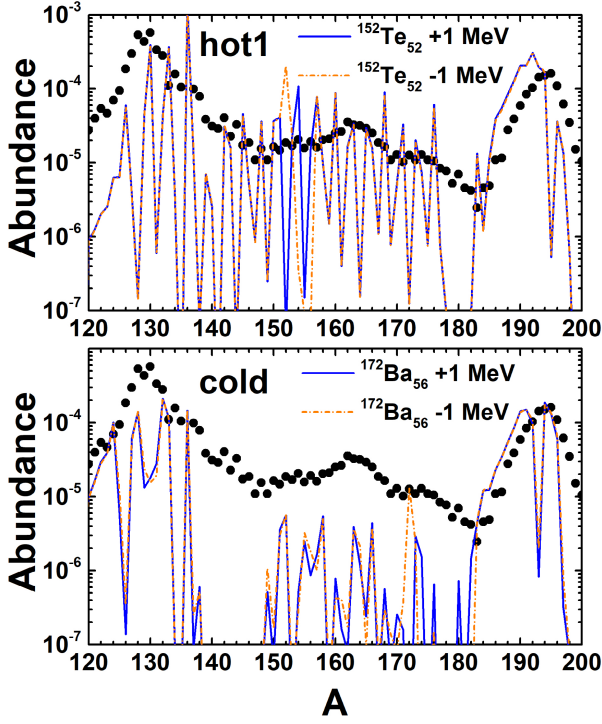


Fig. 2. (color online) Abundance distributions at the time of the r -process freeze-out following nuclear mass variation in the *hot1* and *cold* scenarios. The solid blue line represents the abundance distribution resulting from a mass increase of 1 MeV, while the dotted orange line corresponds to the abundance distribution resulting from a mass decrease of 1 MeV. The dots represent the solar r -process abundance pattern [33].

results are presented in Figs. 3 and 4, where the left panels display the sensitivity measures and the right panels present the corresponding abundance distributions at the r -process freeze-out. The results indicate that, in the four considered scenarios, region I corresponded to the region through which the nuclear flow passed at freeze-out. In the *cold* scenario, the nuclear flow extended farther from stability compared with the hot r -process conditions. It can be clearly observed that nuclei with high sensitivity were distributed along the r -process freeze-out path, implying that mass variations of nuclei in this region strongly impacted the abundance distribution at freeze-out across all four scenarios.

In the *hot1* scenario, differences in the abundance distribution at freeze-out propagated through the later stage of nucleosynthesis, leading to significant variations in the final abundance pattern. However, in the *hot2* and *cold* scenarios, even though mass variations of certain nuclei in region I caused considerable differences in the abundance distribution at freeze-out, their impact on the final abundance pattern was minimal or negligible. This is primarily owing to the influence of fission fragments, which play an important role in shaping the rare-earth peak abundances. We calculated the contribution of fission products to the abundance in the *cold* scenario as an example to prove this point, as follows:

$$\Delta Y_{\text{Fragment}}(A) = \sum_n \sum_i f_i^{(n)} \times w_i(A). \quad (3)$$

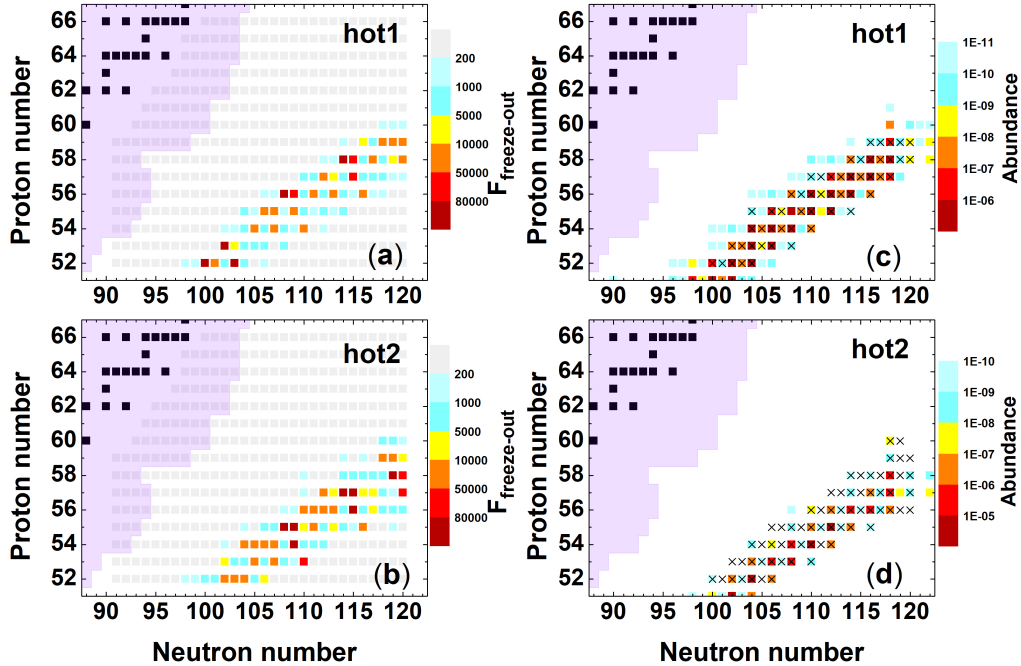


Fig. 3. (color online) In the *hot1* and *hot2* scenarios, panels (a) and (b) correspond to the sensitivity measure $F_{\text{freeze-out}}$ of the abundance distribution at the r -process freeze-out to nuclear masses, whereas panels (c) and (d) correspond to the abundance distribution patterns at freeze-out. Nuclei with $F_{\text{freeze-out}}$ values greater than 1000 are represented by a cross in panels (c) and (d).

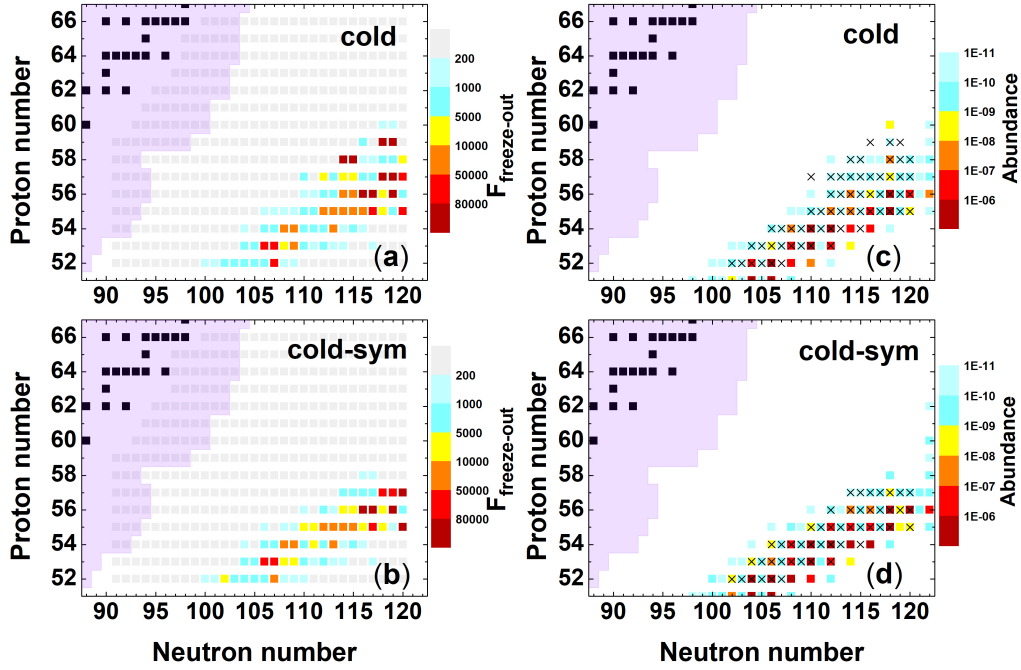


Fig. 4. (color online) As in Fig. 3, but with results for the *cold* and *cold-sym* scenarios.

We took the integrated fission flow $f_i^{(n)}$ of a parent nucleus n , multiplied it by the fission yield $w_i(A)$ of the corresponding fission product with mass number A , and then summed the contributions from all fissioning nuclei, where i refers to a certain fission channel. $\Delta Y_{\text{Fragment}}$ represents the increase in the abundance of nuclei with mass number A owing to fission deposition. Details of the relevant physical quantities can be found in Ref. [29]. The calculated contribution of the fission fragments to the abundance is shown in Fig. 5. The results indicate that when using the GEF model, a significant number of fission fragments were distributed within the rare-earth peak mass region. In the *hot2* and *cold* scenarios, the overall abundance in the rare-earth peak region was very low at freeze-out. However, as nucleosynthesis progresses, a substantial amount of fission fragments was deposited in this region, gradually increasing abundance in the rare-earth region. The contribution of fission fragments diminished the variations in the rare-earth peak abundance distribution that were initially caused by nuclear mass changes. As a result, the impact of mass variations in region I was masked by the distribution of fission fragments, leading to a generally lower sensitivity measure F for nuclei in this region. In contrast, in the *cold-sym* scenario, where symmetric fission treatment was applied, fission fragments were only deposited near the second r -process peak, as indicated by the blue squares in Fig. 5. In the absence of a direct contribution of fission fragments to the rare-earth region, the differences in the abundance at freeze-out caused by mass variations in region I persisted and ultimately influenced the final rare-earth peak abundance distribution. Thus, the sensitivity of

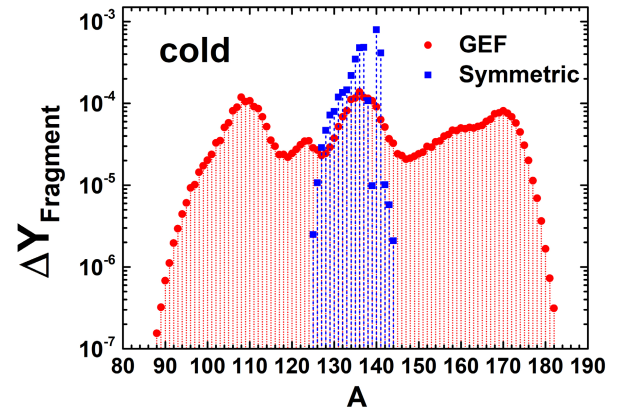


Fig. 5. (color online) Contribution of fission fragments to the abundance distribution in the *cold* scenario. The red dots represent the increase in abundance due to fission deposition when using the GEF fission fragment distribution model, while the blue squares represent the contribution of fission fragments under the simple symmetric fission treatment.

region I increased again. However, the solar rare-earth peak abundance cannot be reproduced using the symmetric fission treatment.

When the r -process nuclear flow reached region II, the rare-earth peak was essentially fully formed, and its shape was highly sensitive to mass variations of nuclei in this region, which were located along the r -process path when $\tau_{n\gamma} \approx 3\tau_\beta$. As mentioned previously, in the *hot2* and *cold* scenarios, the contribution of fission products eliminated the high sensitivity of nuclei along the early r -process path (region I). However, in the process of nuclear flow decay back to stability, the fission flow will gradu-

ally decrease over time, which means that the contribution of fission fragments to the rare-earth peak abundance will gradually decrease. We calculated the contribution of fission products to rare-earth peak abundances over time in the *cold* scenario, as shown in Fig. 6. $\Delta Y_F(t)$ is defined as

$$\Delta Y_F(t) = \sum_{A=150}^{178} \sum_n \sum_i F_i^{(n)}(t) \times w_i(A), \quad (4)$$

where $F_i^{(n)}(t)$ is the fission flow of a parent nucleus n at a certain moment t , and $w_i(A)$ is the fission yield. We summed the contributions from all fissioning nuclei to the rare-earth mass region $A = 150 - 178$. $\Delta Y_F(t)$ represents the increase in the abundance of nuclei with $A = 150 - 178$ owing to fission deposition. The results show that, following the *r*-process freeze-out, the contribution of fission to the rare-earth peak gradually decreased. For nuclei in region I, which were produced around the time of the *r*-process freeze-out, the strong deposition of fission products started to take effect at this stage and eventually erased the mass sensitivities. However, as the nuclear flow reached region II at a later time, the contribution of fission gradually decreased, and hence, the weakening effect of fission fragments on the difference of the abundance distribution weakened. Therefore, the nuclei in region II still had larger F values. In addition, we note a distinct spike in the contribution of fission fragments at approximately 0.5 s in Fig. 6. This evolution closely follows the time-dependent behavior of the fission flow $F_i^{(n)}(t)$, and the observed feature resulted from two combined effects. First, the neutron-to-seed ratio decreased rapidly and fell below 1.0 around the time of the *r*-process freeze-out (~ 0.48 s). The sudden reduction in the free neutron population led to a sharp decline in neutron-induced fission. Following freeze-out, β -delayed neutron emission provided additional free neutrons, reviving the neutron-induced fission flow and contributing to the subsequent increase in the total fission flow. Second, β -delayed fission primarily occurred following freeze-out. As the relevant nuclei decayed and underwent β -delayed fission, their contribution to the total fission flow became significant [29]. These two effects together led to the second hump observed at approximately 0.5 s in both the total fission flow and the contribution of fission fragments to the rare-earth peak abundances.

IV. SUMMARY

Based on the results of sensitivity studies in our previous work [24], we further analyzed the underlying reasons for the different distribution patterns of high-sensitivity nuclei across various astrophysical scenarios. The res-

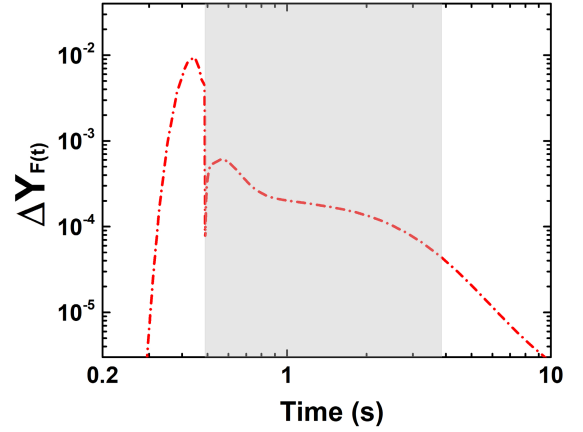


Fig. 6. (color online) Evolution of the contribution of fission fragments to the rare-earth peak abundances over time in the *cold* scenario. The shaded area represents the time interval for the formation of the rare-earth peak, from the time of the *r*-process freeze-out to the time when the neutron capture timescale $\tau_{n\gamma}$ was approximately equal to three times the β -decay timescale τ_β .

ults showed that the mass variations of nuclei in region I (20–30 neutrons away from stability) had a significant impact on the abundance distribution at the *r*-process freeze-out across all four scenarios, highlighting the universality of their influence at this stage. However, in scenarios with extensive fission activity, the subsequent deposition of fission products into the rare-earth region started to take effect following freeze-out. Fission deposition effectively reset the local abundances in this region and suppressed the sensitivity to nuclear masses along the *r*-process freeze-out path. This process significantly reduced the uncertainty in the rare-earth peak abundances caused by mass variations in region I, producing a more robust *r*-process abundance distribution.

With time evolution, the fission flow in the *r*-process nucleosynthesis gradually declined, leading to a reduced contribution from fission deposition. As the *r*-process path moved towards stability at a later time, the weakening effect of fission fragments on the difference in the abundance distribution weakened. Consequently, the sensitivity of nuclear masses in region II (7–15 neutrons away from stability) remained less affected by fission fragments, allowing nuclei in this region to retain relatively high sensitivity. This study highlights the impact of fission on the sensitivity of *r*-process abundances to nuclear masses, contributing to a better understanding of rare-earth peak formation and improving its effectiveness as a diagnostic for the *r*-process site.

ACKNOWLEDGEMENTS

The authors also want to thank the fruitful discussions with Prof. F. Q. Chen and Dr. W. L. Lv.

References

- [1] E. M. Burbidge, G. R. Burbidge, W. A. Fowler *et al.*, *Rev. Mod. Phys.* **29**, 547 (1957)
- [2] K. Marti and H. D. Zeh, *Meteoritics* **20**, 311 (1985)
- [3] J. J. Cowan, C. Sneden, J. E. Lawler *et al.*, *Rev. Mod. Phys.* **93**, 015002 (2021)
- [4] X. D. Xu, B. Sun, Z. M. Niu *et al.*, *Phys. Rev. C* **87**, 015805 (2013)
- [5] D. Martin, A. Arcones, W. Nazarewicz *et al.*, *Phys. Rev. Lett.* **116**, 121101 (2016)
- [6] M. Mumpower, R. Surman, G. McLaughlin *et al.*, *Prog. Part. Nucl. Phys.* **86**, 86 (2016)
- [7] Z. Li, Z. Niu, and B. Sun, *Sci. Chin. Phys., Mech. Astron.* **62**, 982011 (2019)
- [8] T. M. Sprouse, R. Navarro Perez, R. Surman *et al.*, *Phys. Rev. C* **101**, 055803 (2020)
- [9] J. Chen, J. Y. Fang, Y. W. Hao *et al.*, *Astrophys. J.* **943**, 102 (2023)
- [10] Y.-W. Hao, Y.-F. Niu, and Z.-M. Niu, *Phys. Rev. C* **108**, L062802 (2023)
- [11] R. Surman, J. Engel, J. R. Bennett *et al.*, *Phys. Rev. Lett.* **79**, 1809 (1997)
- [12] M. R. Mumpower, G. C. McLaughlin, and R. Surman, *Phys. Rev. C* **85**, 045801 (2012)
- [13] M. R. Mumpower, G. C. McLaughlin, and R. Surman, *Astrophys. J.* **752**, 117 (2012)
- [14] M. Mumpower, R. Surman, D. L. Fang *et al.*, *J. Phys. G: Nucl. Part. Phys.* **42**, 034027 (2015)
- [15] M. R. Mumpower, R. Surman, D.-L. Fang *et al.*, *Phys. Rev. C* **92**, 035807 (2015)
- [16] X. F. Jiang, X. H. Wu, and P. W. Zhao, *Astrophys. J.* **915**, 29 (2021)
- [17] S. Brett, I. Bentley, N. Paul *et al.*, *Eur. Phys. J. A* **48**, 184 (2012)
- [18] A. Aprahamian, I. Bentley, M. Mumpower *et al.*, *AIP Advances* **4**, 041101 (2014)
- [19] J. Beun, J. C. Blackmon, W. R. Hix *et al.*, *J. Phys. G: Nucl. Part. Phys.* **36**, 025201 (2008)
- [20] R. Surman, J. Beun, G. C. McLaughlin *et al.*, *Phys. Rev. C* **79**, 045809 (2009)
- [21] M. R. Mumpower, G. C. McLaughlin, and R. Surman, *Phys. Rev. C* **86**, 035803 (2012)
- [22] R. Surman, M. Mumpower, J. Cass *et al.*, *EPJ Web Conf.* **66**, 07024 (2014)
- [23] M. Mumpower, J. Cass, G. Passucci *et al.*, *AIP Advances* **4**, 041009 (2014)
- [24] Y. W. Hao, Y. F. Niu, and Z. M. Niu, *Phys. Lett. B* **844**, 138092 (2023)
- [25] <https://sourceforge.net/projects/nucnettools/>
- [26] P. Moller, J. Nix, W. Myers *et al.*, *Atom. Data. Nucl. Data Tables* **59**, 185 (1995)
- [27] <https://tendl.web.psi.ch/tendl2019/talys.html>
- [28] <https://reaclib.jinaweb.org/>
- [29] Y. W. Hao, Y. F. Niu, and Z. M. Niu, *Astrophys. J.* **933**, 3 (2022)
- [30] <http://www.cenbg.in2p3.fr/GEF>
- [31] N. Vassh, R. Vogt, R. Surman *et al.*, *J. Phys. G: Nucl. Part. Phys.* **46**, 065202 (2019)
- [32] M. Wang, W. Huang, F. Kondev *et al.*, *Chin. Phys. C* **45**, 030003 (2021)
- [33] C. Sneden, J. J. Cowan, and R. Gallino, *Ann. Rev. Astron. Astrophys.* **46**, 241 (2008)